

Macroscopic Resonant Tunneling through Andreev Interferometers

M.C. Goorden

Département de Physique Théorique, Université de Genève, CH-1211 Genève 4, Switzerland

Ph. Jacquod and J. Weiss

Physics Department, University of Arizona, 1118 E. 4th Street, Tucson, AZ 85721, USA

(Dated: October 29, 2018)

We investigate the conductance through and the spectrum of ballistic chaotic quantum dots attached to two s -wave superconductors, as a function of the phase difference ϕ between the two order parameters. A combination of analytical techniques – random matrix theory, Nazarov’s circuit theory and the trajectory-based semiclassical theory – allows us to explore the quantum-to-classical crossover in detail. When the superconductors are not phase-biased, $\phi = 0$, we recover known results that the spectrum of the quantum dot exhibits an excitation gap, while the conductance across two normal leads carrying N_N channels and connected to the dot via tunnel contacts of transparency Γ_N is $\propto \Gamma_N^2 N_N$. In contrast, when $\phi = \pi$, the excitation gap closes and the conductance becomes $G \propto \Gamma_N N_N$ in the universal regime. For $\Gamma_N \ll 1$, we observe an order-of-magnitude enhancement of the conductance towards $G \propto N_N$ in the short-wavelength limit. We relate this enhancement to resonant tunneling through a macroscopic number of levels close to the Fermi energy. Our predictions are corroborated by numerical simulations.

PACS numbers: 74.45.+c, 73.23.-b, 74.78.Na, 05.45.Mt

I. INTRODUCTION

Andreev reflection plays a central role in the description of hybrid nanostructures with both superconducting and normal components [1]. The process is illustrated in Fig. 1. When a negatively charged electron in the normal metal hits the interface with a superconductor, it is retroreflected into a positively charged hole. The superconductor acts as a charge-inverting mirror, which leads to a variety of intriguing effects in transport and spectroscopy of hybrid nanostructures [2]. Here, we show how Andreev reflection resonantly enhances the tunneling conductance through a quantum dot by orders of magnitude, when the dot is coupled to two superconductors with phase difference $\phi = \pi$ between their order parameters. The effect quickly disappears as ϕ is tuned away from resonance and might have applications in low-temperature current switching devices and magnetic flux “transistors”, where ϕ would be controlled by an external magnetic flux.

In a chaotic Andreev billiard, an impurity-free quantum dot coupled to one or more superconductors, Andreev reflection renders all orbits periodic near the Fermi level [3]. Periodic orbits consist of an electron and a hole retracing each other’s path, and therefore touching the superconductor at both ends. This fact suggests that the density of states of an Andreev billiard can be determined by Bohr-Sommerfeld quantization. For a single superconducting lead, this results in a density of states which is exponentially suppressed for low energies, on the scale of the Thouless energy $E_{T,S} = \hbar/2\tau_{D,S}$, where $\tau_{D,S}$ is the average time between Andreev reflections [4, 5]. Simultaneously, one expects random matrix theory (RMT) to be valid for chaotic quantum dots [6]. RMT however leads to a different prediction, that a hard gap in the

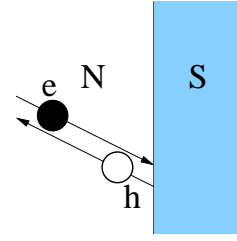


Figure 1: Andreev reflection by a superconductor (S). An incoming electron (e) in a normal metal (N) near the Fermi energy E_F is reflected as a hole (h) with opposite velocity.

density of states opens up at an energy $E_0 \simeq 0.6E_{T,S}$ [4]. It was realized in Ref. [7] that the discrepancy between the theories was not a short-coming in one of them but indicates that they have different regimes of validity. The crossover between the two regimes is determined by the Ehrenfest time, which is the time scale for an initially minimal wave packet to spread over the system. For a closed chaotic billiard of linear size L_c and Lyapunov exponent λ , the Ehrenfest time reads $\tau_E = \lambda^{-1} \ln[k_F L_c]$, with the Fermi wavenumber k_F of the quasiparticles [8].

RMT is valid in the *universal regime* of vanishing Ehrenfest time, $\tau_E \ll \tau_{D,S}$, while Bohr-Sommerfeld quantization gives a good description in the opposite *semiclassical regime*, $\tau_E \gg \tau_{D,S}$. Previous investigations of the crossover from the RMT regime to the semiclassical regime in Andreev billiards have considered the density of states in the presence of a single s -wave superconductor, focusing on the reduction of the excitation gap in the semiclassical regime, as well as its fluctuations [8, 9, 10, 11, 12, 13, 14, 15, 16, 17, 18, 19]. The Ehrenfest time effects are usually small and it takes a

large computational effort to extract them numerically.

In this article we investigate transport via normal metallic leads through an Andreev billiard connected to two ϕ -biased superconductors. The system we consider is shown in Fig. 2. A chaotic quantum dot with mean level spacing δ is coupled to two superconductors. The superconducting lead 1 (2) has order parameter $\Delta_0 e^{i\phi_1}$ ($\Delta_0 e^{i\phi_2}$), and we take $\Delta_0 \in \mathcal{R}$. One way to control the phase difference $\phi \equiv \phi_1 - \phi_2$ is to have them form a loop, which one then threads with a magnetic flux Φ – this is sketched in Fig. 2. Alternatively, the phase difference can be generated by a supercurrent. In this case $\phi \equiv \phi_1 - \phi_2 = 2\pi\Phi/\Phi_0$, in terms of the flux quantum $\Phi_0 = h/2e$. Since any global phase can be gauged out, we set $\phi_1 = \phi/2$ and $\phi_2 = -\phi/2$. We assume that each superconducting lead has N_S channels connected to the quantum dot via tunnel contacts with tunnel probability Γ_S . The average time $\tau_{D,S} = \hbar/2E_{T,S}$ between Andreev reflections is associated with the superconducting Thouless energy $E_{T,S} = 2N_S\Gamma_S\delta/4\pi$. Quasiparticle excitations have energy E measured from the Fermi energy E_F , with $|E| \ll \Delta_0$. Thus the quasiparticles cannot penetrate into the superconductors. We also assume $\Delta_0 \ll E_F$, in which case Andreev reflection perfectly retroreflects electrons into holes and vice versa, with a phase shift $-\pi/2 \pm \phi_i$. At $\phi = 0$, this *Andreev phase* shift is solely due to the penetration of the wavefunction into the superconductor. The additional phase shift $\pm\phi_i$ is due to the global phase of the superconductor at contact i , where the minus sign is for reflection from electron to hole, and the plus sign for reflection from hole to electron. We will refer to the quantum dot with two superconducting leads (but no normal lead) as the closed Andreev billiard. For the transport set-up we connect the quantum dot to two external normal leads through a tunnel contact with tunnel probability Γ_N . The current is measured between the right (R) and left (L) lead, which both carry N_N transport channels.

The combination of Andreev and Ehrenfest physics in such an *Andreev interferometer* gives rise to an order-of-magnitude enhancement of the tunneling conductance when $\phi = \pi$. In the tunneling regime $\Gamma_N \rightarrow 0$, the conductance is strongly affected by the density of states of the closed Andreev billiard. In the absence of superconductivity ($\Gamma_S = 0$) and for $\Gamma_N N_N \gtrsim 1$ (we restrict ourselves to that regime to avoid Coulomb blockade effects), the conductance is just the classical series conductance $G = G_0\Gamma_N N_N/2 + \mathcal{O}(1)$, where $G_0 = 2e^2/h$ [20]. In contrast, we will see below that in the limit $\tau_E/\tau_D \sim 1$, and for well coupled superconductors, $\Gamma_S \simeq 1$, the conductance at $\phi = \pi$ becomes $G \propto G_0 N_N$. We identify the mechanism behind this enhancement as *macroscopic resonant tunneling* through a large number of low-energy quasi-degenerate Andreev levels very close to the Fermi energy. Indeed, for $\phi = \pi$, all periodic trajectories touching both superconductors, irrespective of their lengths, contribute to the density of states at the Fermi energy in the semiclassical regime. Such a large

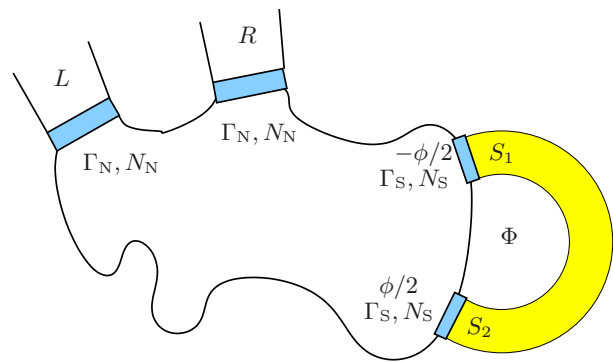


Figure 2: Quantum dot doubly coupled to a superconducting ring. Both contact to the superconductor have N_S channels and tunneling probability Γ_S . The flux threading the ring causes a phase difference $\phi = 2\pi\Phi/\Phi_0$ between the two superconducting contacts. Transport through the structure is investigated between two external normal leads (L and R), each carrying N_N transport channels, with tunnel contact of tunnel probability Γ_N .

effect is already clearly visible for moderate Ehrenfest time, in contrast to previous works which found rather small manifestations of Ehrenfest physics for larger τ_E/τ_D [9, 10, 11, 12, 13, 14, 15, 16]. While similar behaviors were reported for cavities without transport [21] or internal [22] mode-mixing, this effect was not found in earlier analytical works on transport through chaotic Andreev interferometers [23, 24, 25, 26].

The paper is organized as follows. In section II we calculate the density of states of the closed Andreev billiard. We repeat previous results in the RMT limit and calculate the Bohr-Sommerfeld density of states as a function of ϕ . We show that due to a special resonance condition, the density of states for phase differences close to π has a large peak around the Fermi energy. We proceed with a calculation of the conductance in Section III. In the RMT limit we use Nazarov’s circuit theory [27, 28]. For weakly coupled normal leads, we find that the conductance is small, $\propto \Gamma_N^2 N_N$, for $\phi \ll \pi$, while it reaches the classical series conductance for $\phi = \pi$, because of the disappearance of the gap in the density of states. In the semiclassical limit we employ a semiclassical trajectory-based method [29, 30, 31, 32, 33]. We find that the large peak in the density of states at the Fermi level has its counterpart in the conductance, which is a factor $1/\Gamma_N \gg 1$ larger than in the RMT limit. In section IV, numerical simulations confirm the validity of our analytical results.

II. SPECTRUM OF ANDREEV BILLIARDS

A. Random matrix theory

The density of states in the universal regime has been calculated in Refs. [4, 17] using RMT. We repeat the

main steps of the calculation for $\Gamma_S = 1$, and refer the reader to Refs. [4, 34] for the calculation at arbitrary Γ_S . At low excitation energy $E \ll \Delta_0$, the spectrum of Andreev billiards is most conveniently obtained from the low-energy effective Hamiltonian [34]

$$\mathcal{H} = \begin{pmatrix} H & -\pi WW^T \\ -\pi WW^T & -H^* \end{pmatrix}, \quad (1a)$$

$$W_{mn} = \delta_{mn} \left(\frac{M\delta}{\pi^2} \right)^{1/2}, \quad (1b)$$

$$m = 1, 2, \dots, M, \quad n = 1, 2, \dots, 2N_S,$$

which is constructed from the quantum dot's one-quasiparticle $M \times M$ Hamiltonian matrix H and the projection matrix WW^T giving the coupling between the quantum dot and the superconductors. We define a 2×2 Green function $G(z)$ from the matrix Green function $\mathcal{G}(z) = \langle (z - \mathcal{H})^{-1} \rangle$

$$G = \begin{pmatrix} G_{11} & G_{12} \\ G_{21} & G_{22} \end{pmatrix} = \frac{\delta}{\pi} \begin{pmatrix} \text{Tr}\mathcal{G}_{11} & \text{Tr}\mathcal{G}_{12} \\ \text{Tr}\mathcal{G}_{21} & \text{Tr}\mathcal{G}_{22} \end{pmatrix}, \quad (2)$$

from which the density of states reads

$$\rho_{\text{RMT}}(E) = -\frac{2}{\delta} \text{Im}[G_{11}(E + i0^+)]. \quad (3)$$

Here, G_{11} is self-consistently determined by the equations

$$G_{11}(z) = -\frac{2\pi z}{N_S \delta} \left(G_{12}^2(z) + \frac{G_{12}(z)}{\cos(\phi/2)} \right), \quad (4a)$$

$$G_{12}^2(z) = 1 + G_{11}^2(z). \quad (4b)$$

For $\phi = 0$, the density of states has a gap at an energy $E_0 \approx 0.6E_{T,S}$. The energy of the gap is reduced when ϕ is increased, closing at a value $\phi = \pi$, where one finds a flat density of states $\rho(E) = 2/\delta$.

The theory of Refs. [4, 17] is only valid for energies larger than the level spacing δ . For a phase difference $\phi = \pi$, the system belongs to the symmetry class CI of Ref. [35], and the density of states reads

$$\rho(E) = \frac{\pi}{\delta} \int_0^{2\pi E/\delta} dt J_0(t) J_1(t)/t, \quad (5)$$

with Bessel functions J_0 and J_1 . This prediction retains its validity down to low excitations $E < \delta$. For energies $E \gg \delta$ (but still $E \ll \Delta_0$), Eq. (5) reduces to the mean field theory and gives $\rho(E) = 2/\delta$, while for $E \lesssim \delta$ it predicts a linearly vanishing density of states $\rho(E) = \pi^2 E/\delta$.

B. Semiclassical regime

The retroreflection at the superconductor makes all classical trajectories near the Fermi level periodic [3]. The elements of a periodic trajectory are an electron and a hole segment retracing each other, and touching a superconducting contact at both ends. The phase accumulated along a periodic orbit of period T in one period consists of (i) the phase $2ET/\hbar$ acquired during the motion in the normal region and (ii) the phase shift acquired at the two Andreev reflections. This shift equals $-\pi$ if the two reflections take place at the same superconducting lead and $-\pi \pm \phi$ if they take place at different superconductors. Summing the different contributions and requiring that the phase accumulated in one period is a multiple of 2π leads to the Bohr-Sommerfeld quantization conditions

$$E_n = \pi\hbar(n + 1/2) / T, \quad (6a)$$

$$E_n = \pi\hbar(n + 1/2 + \phi/2\pi) / T, \quad (6b)$$

$$E_n = \pi\hbar(n + 1/2 - \phi/2\pi) / T. \quad (6c)$$

Eq. (6a) applies to trajectories touching the same superconductor twice, while Eqs. (6b) and (6c) to trajectories touching both superconductors, depending on whether the Andreev reflection from electron to hole takes place at the superconductor with phase $\phi/2$ [Eq. (6b)] or $-\phi/2$ [Eq. (6c)]. Assuming ergodicity, the corresponding trajectories have a weight $1/2, 1/4, 1/4$, leading to a mean density of states (see also Ref. [36] for a single superconducting contact)

$$\rho_{\text{BS}}(E) = N_S \int_0^\infty dT P(T) \sum_n \left[\delta \left(E - [n + \frac{1}{2}] \frac{\pi\hbar}{T} \right) + \frac{1}{2} \delta \left(E - [n + \frac{1}{2} + \frac{\phi}{2\pi}] \frac{\pi\hbar}{T} \right) + \frac{1}{2} \delta \left(E - [n + \frac{1}{2} - \frac{\phi}{2\pi}] \frac{\pi\hbar}{T} \right) \right]. \quad (7)$$

Here $P(T)$ is the classical distribution of return times to a superconducting contact. Inserting the chaotic distribution $P(T) = \exp(-T/\tau_{D,S})/\tau_{D,S}$ into Eq. (7) gives

$$\rho_{\text{BS}}(u) = \frac{2\pi}{\delta} \frac{\cosh\left(\frac{\phi}{2u}\right)}{\sinh\left(\frac{\pi}{u}\right)u^2} \left(\pi \cosh\left(\frac{\phi}{2u}\right) \coth\left(\frac{\pi}{u}\right) - \phi \sinh\left(\frac{\phi}{2u}\right) \right), \quad (8)$$

with $u = E/E_{T,S}$. For $\phi = 0$ Eq. (8) reduces to the Bohr-Sommerfeld approximation of Refs. [4, 5] and the density of states is exponentially suppressed at low energies.

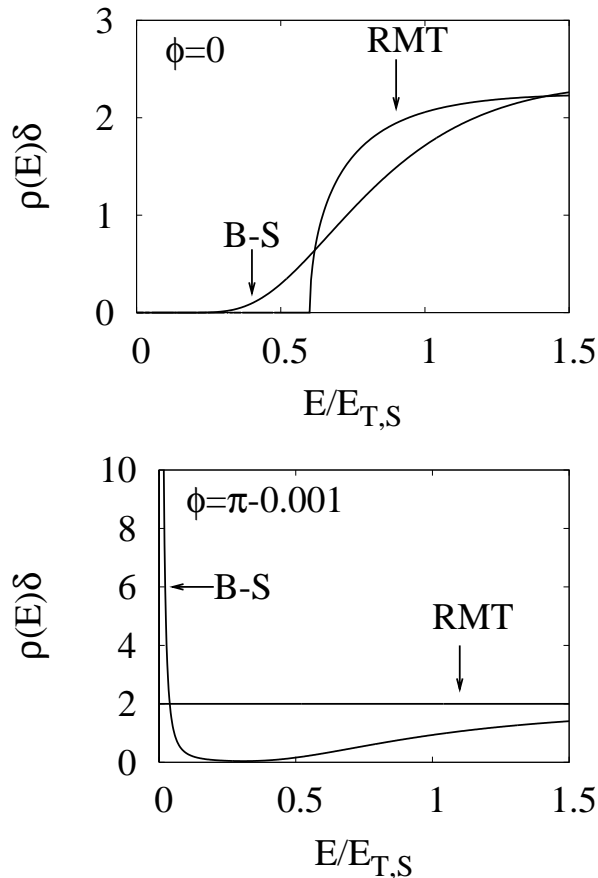


Figure 3: Comparison of the density of states calculated from Bohr-Sommerfeld quantization and random matrix theory (RMT). The top panel is for a phase difference $\phi = 0$, and the bottom panel for $\phi \approx \pi$.

C. Comparison of the two regimes

The low energy approximation of Eq. (8) reads

$$\lim_{u \rightarrow 0} \rho_{BS}(u) = \frac{2\pi}{\delta} \frac{e^{-(\pi-\phi)/u} (\pi - \phi)}{2u^2}. \quad (9)$$

For $\pi - \phi \ll 1$ this gives a sharply peaked function with a maximum value of $\rho_{BS} = \frac{4\pi}{e^2(\pi-\phi)}$ at energy $u = \frac{\pi-\phi}{2}$. In the limit $\phi \rightarrow \pi$ we find

$$\lim_{u \rightarrow 0} \lim_{\phi \rightarrow \pi} \rho_{BS}(u) = \frac{2\pi}{\delta} \delta(u). \quad (10)$$

Eq. (10) predicts a number $\mathcal{O}[N_S]$ of levels around $E = 0$. The peculiar behavior at $\phi = \pi$ is due to the fact that the two quantization conditions (6b) and (6c) have solutions $E = 0$ simultaneously for *all* trajectories, irrespective of their period.

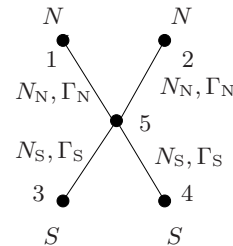


Figure 4: Circuit for our system. We have two normal electrodes (1, 2), two superconducting electrodes (3, 4) and one internal junction, the chaotic cavity (5). The superconducting (normal) leads have N_S (N_N) channels with transmission probability Γ_S (Γ_N).

Fig. 3 illustrates the predictions of the previous two paragraphs. In the RMT limit we combine the solution of Eqs. (4a) and (4b) with Eq. (3), while in the semiclassical limit we use Eq. (7). For $\phi = 0$ (top panel), the density of states in the RMT and semiclassical limit are very similar. Both densities of states are suppressed at the Fermi energy, while they are restored to a value of $2/\delta$ at an energy scale set by $E_{T,S}$. The main difference is in the way that ρ is suppressed: a hard gap in the RMT limit vs. an exponential suppression for the semiclassical density of states.

In contrast, when $\phi \approx \pi$, the difference between RMT and Bohr-Sommerfeld predictions is huge. While in the RMT limit the density of states is flat [up to the minigap of order δ predicted by Eq.(5) which is not resolved in Fig. 3], it shows a large peak around the Fermi energy in the semiclassical limit. For $\phi = \pi$ the peak is described by a Dirac δ -function (cf. Eq. (10)), which is why we show a density of states at a phase difference slightly different from π in Fig. 3.

III. TRANSPORT

A. Random matrix theory

We use Nazarov's circuit theory of Andreev conductance [27] to calculate the two-terminal conductance through the system shown in Fig. 2 (see also Ref. [28]). The theory describes hybrid nanostructures in the same language as electrical circuits: i.e. their structure is reduced to internal junctions, normal/ superconducting external junctions (electrodes) and leads connecting the different elements. The leads are characterized by a set of transmission eigenvalues. The conductance between different electrodes is determined by a simple set of algebraic equations. As the energy dependence of the scat-

tering matrix is neglected, the theory is valid for small temperatures and voltages. The superconductors have the same voltage. The results are valid to leading order in $\Gamma_S N_S$, $\Gamma_N N_N$.

Our system consists of two normal external junctions (denoted by indices 1, 2), two superconducting external junctions 3, 4 and one internal junction, the chaotic cavity 5. This is illustrated in Fig. 4. The calculation of the conductance starts with the assignment of a complex amplitude f_k to each junction. The amplitudes are somewhat analogous to voltages: if a junction n is connected to a junction m by a lead with a large conductance, then $f_n \rightarrow f_m$. The physical meaning of the amplitudes is the following: if electrons are injected into the k^{th} junction via an additional weakly coupled normal electrode, a beam of holes with intensity $|f_k|^2$ times that of the electron beam is retro-reflected into that probe. For the external junctions the value of the amplitudes is prescribed by the theory: for the normal external junctions $f_1, f_2 = 0$ and for the superconducting junctions $f_3 = \exp(-i\phi/2)$, $f_4 = \exp(i\phi/2)$. The amplitude f_5 can be found by the spectral current conservation rule [28]. One has $f_5 = \tan(\theta_5/2)$, with θ_5 to be determined by

$$\frac{\Gamma_S N_S}{\Gamma_N N_N} \cos \frac{\phi}{2} \cos \theta_5 (1 + \cos \theta_5) \left(1 + (1 - \Gamma_N) \tan^2 \frac{\theta_5}{2} \right) = \sin \theta_5 (2 - \Gamma_S + \Gamma_S \sin \theta_5 \cos \frac{\phi}{2}). \quad (11)$$

Once the complex amplitudes are known, the RMT-averaged conductance between junctions 1 and 2 is given by

$$\langle G \rangle / G_0 = \frac{\Gamma_N N_N \cos \theta_5 + \Gamma_N \sin^2[\theta_5/2]}{2 (1 - \Gamma_N \sin^2[\theta_5/2])^2}. \quad (12)$$

The self-consistency equation (11) for θ_5 combined with Eq. (12) determines the conductance. For ballistic leads ($\Gamma_N = \Gamma_S = 1$) we reproduce the results of Ref. [25].

Of most interest to us is the regime $\Gamma_N \ll 1$ and $\Gamma_S = 1$, where we expect a strong connection between conductance and density of states. In the limit $\delta\phi = \pi - \phi \gg \Gamma_N$, we use an expansion in terms of Γ_N , while in the opposite limit, we first expand in the small parameter $\delta\phi$. From Eqs. (11) and (12) we find, to leading order in Γ_N ,

$$\langle G \rangle / G_0 = \begin{cases} \Gamma_N^2 N_N \left(1 + \frac{N_N}{N_S} \frac{1 + \cos \frac{\phi}{2}}{\cos \frac{\phi}{2}} \right) / 4, & \text{if } \delta\phi \gg \Gamma_N, \\ \Gamma_N N_N / 2 + \mathcal{O}(\delta\phi^2), & \text{if } \delta\phi \ll \Gamma_N. \end{cases} \quad (13)$$

The main feature of Eq. (13) is that, for $\phi = \pi$, one has the same conductance as a two-terminal quantum dot without superconductor. This result agrees with the density of states where the influence of the superconductors also disappears and the density of states becomes flat (bottom panel of Fig. 3). The minigap of magnitude δ is hardly resolved, due to the coupling to external

leads and the associated broadening of levels. On the other hand, for $\phi \neq \pi$ the density of states is strongly suppressed at the Fermi level (top panel of Fig. 3) and we expect a conductance which is reduced due to the presence of the superconductors. Eq. (13) does indeed predict a conductance of order Γ_N^2 .

From Eq. (13) it follows that the crossover between the two limits occurs when $\delta\phi = \Gamma_N N_N / N_S$. We now connect this to the density of states of the Andreev billiard. Taylor expanding Eqs. (3), (4a) and (4b) in $\delta\phi$ gives a gap in the density of states at an energy

$$E_0 = \delta\phi E_{T,S} = \delta\phi \frac{N_S \delta}{2\pi}. \quad (14)$$

The density of states of the closed cavity is broadened due to the coupling to normal leads. The coupling to leads results in a non-hermitian Hamiltonian $H \rightarrow H - i\pi W_N W_N^\dagger$, with H the Hamiltonian of the closed system and W_N an $M \times 2N_N$ matrix describing the coupling to the normal leads [20, 37]. The $2N_N \times 2N_N$ matrix $W_N^\dagger W_N$ has eigenvalues $w = \Gamma_N M \delta / 4\pi^2 + \mathcal{O}(\Gamma_N^2)$. For the broadening we need the eigenvalues of the $M \times M$ matrix $W_N W_N^\dagger$. Assuming that all levels in the dot are coupled to the leads in the same manner, we multiply w by $2N_N/M$ to estimate the broadening as $\delta E = 2\pi w N_N / M = \Gamma_N N_N \delta / 2\pi$. Comparing this with Eq. (14) we find that $\delta E = E_0$ for $\Gamma_N N_N = N_S \delta\phi$. This gives the crossover energy scale for Eqs. (13). We conclude that the conductance is not affected by the presence of the superconductors once the gap in the broadened density of states closes.

We finally comment on the effect of a finite tunnel barrier with $\Gamma_S < 1$ between the superconductor and normal metal. For $\Gamma_N \ll 1$, Eq. (12) becomes

$$\langle G \rangle / G_0 = \begin{cases} \Gamma_N^2 N_N \left(1 + \frac{N_N}{N_{S,\text{eff}}} \frac{1 + \cos \frac{\phi}{2}}{\cos \frac{\phi}{2}} \right) / 4, & \text{if } \delta\phi \gg \Gamma_N, \\ \Gamma_N N_N / 2 + \mathcal{O}(\delta\phi^2), & \text{if } \delta\phi \ll \Gamma_N. \end{cases} \quad (15)$$

Here, $N_{S,\text{eff}} = c \Gamma_S N_S$ where $c \in (\frac{1}{2}, 1)$ is a numerical factor depending only weakly on ϕ and Γ_S . A finite Γ_S thus reduces the number of effective superconducting channels to $N_{S,\text{eff}}$.

B. Semiclassical regime

The starting point of our semiclassical treatment is the two-terminal conductance through a metallic system in contact with superconductors (see Fig. 5) [38],

$$G/G_0 = T_{RL}^{ee} + T_{RL}^{he} + 2 \frac{T_{LL}^{he} T_{RR}^{he} - T_{LR}^{he} T_{RL}^{he}}{T_{LL}^{he} + T_{RR}^{he} + T_{LR}^{he} + T_{RL}^{he}}. \quad (16)$$

We used the transmission probability for a quasi-particle of type $\alpha = e, h$ from the normal lead $i = L, R$ to a quasi-particle of type $\beta = e, h$ into the normal lead $j = L, R$,

$$T_{ji}^{\beta\alpha} = \sum_{m \in i; n \in j} |\tau_{n,j;m,i}^{\beta\alpha}|^2. \quad (17)$$

Here, $\tau_{n,j;m,i}^{\beta\alpha}$ gives the transmission amplitude from channel m in lead i to channel n in lead j . Since we consider a symmetric configuration, where both normal leads carry the same number N_N of channels, all of them coupled to the cavity with the same tunnel probability Γ_N , Eq. (16) simplifies to

$$\langle G \rangle / G_0 = \langle T_{RL}^{ee} \rangle + \langle T_{LL}^{he} \rangle. \quad (18)$$

Eq. (18) gives the ensemble-averaged conductance to leading order in $\Gamma_N N_N \gg 1$.

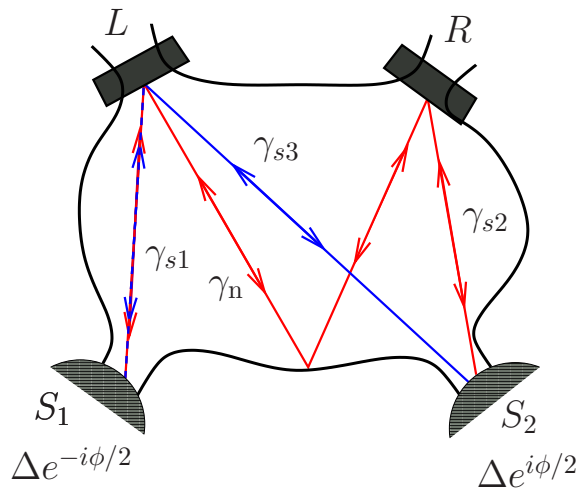


Figure 5: Schematic of the class I (blue) and class II (red) periodic orbits of the closed Andreev billiard, giving rise to macroscopic resonant tunneling at $\phi = \pi$ when the cavity is connected to external electrodes (L and R).

To evaluate the resonant contributions to $\langle T_{RL}^{ee} \rangle$ and $\langle T_{LL}^{he} \rangle$, we follow the semiclassical approach of Ref. [29] (see also Refs. [30, 31, 32, 33]) Semiclassically, the transmission amplitudes read,

$$\tau_{n,j;m,i}^{\beta\alpha} = -(2\pi i \hbar)^{-1/2} \int_i dy_0 \int_j dy \sum_{\gamma} A_{\gamma} \times \langle n|y \rangle \langle y_0|m \rangle \exp[iS_{\gamma}/\hbar + i\pi\mu_{\gamma}/2], \quad (19)$$

where $|m\rangle$ is the transverse wavefunction of the m^{th} lead mode. This expression sums over all trajectories γ (with classical action S_{γ} and Maslov index μ_{γ}) starting at y_0 on a cross-section of the injection (i) lead and ending at y on the exit (j) lead, with even ($\alpha = \beta$) or odd ($\alpha \neq \beta$) number of Andreev reflections. The transmission probabilities are then given by a double sum over trajectories. After the semiclassical approximation that $\sum_n \langle y'|n \rangle \langle n|y \rangle \simeq \delta(y' - y)$ [29] one has

$$T_{ji}^{\beta\alpha} = \frac{1}{2\pi\hbar} \int_i dy_0 \int_j dy'_0 \sum_{\gamma_1, \gamma_2} A_{\gamma_1} A_{\gamma_2}^* \exp[i\delta S/\hbar]. \quad (20)$$

This expression sums over all pairs of classical trajectories γ_1 and γ_2 with fixed endpoints y_0 and y'_0 , which

convert an α quasiparticle into a β quasiparticle. The phase $\delta S = S_{\gamma_1} - S_{\gamma_2}$ gives the difference in action phase accumulated along γ_1 and γ_2 . In the presence of tunnel barriers, the stability amplitudes A_{γ} are given by [33, 39]

$$A_{\gamma} = B_{\gamma} t_i t_j \prod_k [r_k]^{l_{\gamma}(k)}, \quad (21)$$

where $l_{\gamma}(k)$ gives the number of times that γ is reflected back into the system from the tunnel barrier at $k = L, R, S_1$, and S_2 , the transmission and reflection amplitudes satisfy $|t_i|^2 = (1 - |r_i|^2) = \Gamma_{N,S}$ (for $i = L, R, S_1$, or S_2), and $B_{\gamma}^2 = (dp_{y_0}/dy)_{\gamma}$ measures the rate of change of the initial momentum p_{y_0} as the exit position y of γ is changed, for a fixed sequence of transmissions and reflections at the tunnel barriers.

There are four types of trajectories to consider:

- (i) paths that do not touch the superconductors,
- (ii) paths that hit one of the superconductor once,
- (iii) paths that hit the same superconductor twice,
- (iv) paths that hit both superconductors.

Trajectories of type (iv) are flux-dependent. They are depicted in Fig. 5, and it turns out that they are the ones giving rise to macroscopic resonant tunneling. Our semiclassical investigations focus on those paths.

We use Eqs. (20) and (21) to evaluate the dominant semiclassical contributions to Eq. (18). We subdivide the relevant trajectories into class I trajectories, contributing to $\langle T_{LL}^{he} \rangle$ (blue trajectory on Fig.5), and class II trajectories, contributing to $\langle T_{RL}^{ee} \rangle$ (red trajectory on Fig.5).

Class I trajectories are made of the following sequence

$$\gamma_I^{(p)} = \gamma_{s1}^{(e)} + \gamma_{s1}^{(h)} + p \times [\gamma_{s3}^{(h)} + \gamma_{s3}^{(e)} + \gamma_{s1}^{(e)} + \gamma_{s1}^{(h)}], \quad (22)$$

where $s1$ and $s3$ can be interchanged, and $p = 0, 1, 2, \dots$. These trajectories undergo $2p+1$ Andreev reflections and $2p$ reflections at tunnel barriers [40]. They accumulate an action phase

$$S_{\gamma,I} = p(-\pi + \phi + E t_{\ell,I}) + 2 E t_{\gamma_{s1}} - (\pi/2 - \phi/2). \quad (23)$$

One should substitute $\phi \rightarrow -\phi$ when interchanging segments $s1$ and $s3$, though the relative sign between π and ϕ does not affect the final result. Here, $t_{\ell,I}$ gives the duration of the loop [the sequence between bracket in Eq. (22)] and $t_{\gamma_{s1}}$ is the duration of the segment γ_{s1} as shown on Fig. 5. Class II trajectories split into two subclasses, defined by the following two sequences

$$\gamma_{IIa}^{(p)} = \gamma_n^{(e)} \quad (24a)$$

$$+ p \times [\gamma_{s2}^{(e)} + \gamma_{s2}^{(h)} + \gamma_n^{(h)} + \gamma_{s1}^{(h)} + \gamma_{s1}^{(e)} + \gamma_n^{(e)}],$$

$$\gamma_{IIb}^{(p)} = \gamma_{s1}^{(e)} + \gamma_{s1}^{(h)} + \gamma_n^{(h)} + \gamma_{s2}^{(h)} + \gamma_{s2}^{(e)} \quad (24b)$$

$$+ p \times [\gamma_n^{(e)} + \gamma_{s1}^{(e)} + \gamma_{s1}^{(h)} + \gamma_n^{(h)} + \gamma_{s2}^{(h)} + \gamma_{s2}^{(e)}].$$

They undergo $2p$ (IIa) and $2p+2$ (IIb) Andreev reflections, $4p$ (IIa) and $4p+2$ (IIb) reflections at tunnel bar-

riers [40], and accumulate action phases

$$\begin{aligned} S_{\gamma,IIa} &= p(-\pi - \phi + E t_{\ell,IIa}) + (E_F + E) t_{\gamma_n}, \\ S_{\gamma,IIb} &= p(-\pi + \phi + E t_{\ell,IIb}) - (E_F - E) t_{\gamma_n} \\ &\quad + 2E (t_{\gamma_{s1}} + t_{\gamma_{s2}}) - (\pi - \phi). \end{aligned} \quad (25b)$$

Here $t_{\ell,IIa}$ and $t_{\ell,IIb}$ give the duration of the Andreev loops [the two sequences between bracket in Eqs. (24)]. We already see that at $E = 0$ and $\phi = \pi$, the phase difference accumulated by any two members (with different p) of a given family vanishes, so that all pair of trajectories within a given family resonate. There is however no resonance between members of different families.

In normal chaotic billiards, the stability B_γ^2 of periodic orbits decreases exponentially with the number of times the orbit is traveled [41]. The situation is fundamentally different in presence of superconductivity, where Andreev reflections refocus the dynamics. The stability of a tra-

jectory is then only given by the product of the stabilities along the primitive segments, independent of p . We will take these primitive segments as γ_{s1} and γ_{s3} for class I, γ_{s1} , γ_n and γ_{s2} for class II, keeping in mind, however, that the contributions arising from the trajectories of class I and IIa with $p = 0$ are more stable than those with $p \geq 1$, because they do not travel on γ_{s3} (class I) nor on γ_{s1} and γ_{s2} (class IIa). Their contribution is thus underestimated in our approach, and our final results, Eqs. (31) and (32), underestimate the conductance by a subdominant correction.

This enhanced stability applies to trajectories whose Andreev loop is shorter than twice the Ehrenfest time, i.e. the time beyond which an initially narrow wavepacket can no longer fit inside a superconducting lead [7, 9, 12]. The relative measure of trajectories of class I (P_I) and II (P_{II}) is thus

$$P_I(\tau_E/\tau_{D,S}) = \tau_{D,S}^{-2} \int_0^{\tau_E} dt_{s1} \int_0^{\tau_E - t_{s1}} dt_{s3} \exp[-(t_{s1} + t_{s3})/\tau_{D,S}] = 1 - [1 + \tau_E/\tau_{D,S}] \exp[-\tau_E/\tau_{D,S}], \quad (26a)$$

$$\begin{aligned} P_{II}(\tau_E/\tau_{D,S}) &= \tau_{D,S}^{-3} \int_0^{\tau_E} dt_{s1} \int_0^{\tau_E - t_{s1}} dt_n \int_0^{\tau_E - t_{s1} - t_n} dt_{s2} \exp[-(t_{s1} + t_n + t_{s3})/\tau_{D,S}] \\ &= 1 - [1 + \tau_E/\tau_{D,S} + (\tau_E/\tau_{D,S})^2/2] \exp[-\tau_E/\tau_{D,S}]. \end{aligned} \quad (26b)$$

We are now ready to evaluate the dominant contributions to conductance close to resonance. We focus on the low-temperature regime with $E = 0$. We start from Eq. (20) and pair trajectories by class, noting that for a given class, all trajectories have the same stability but differ only by the number of Andreev reflections and normal reflections at the contacts to the normal leads, as well as by the different action phases they accumulate along their Andreev loop. The sum over classes is then represented by a sum over primitive trajectories, and we perform the substitution

$$\sum_{\gamma^1, \gamma^2} A_{\gamma^1} A_{\gamma^2}^* [\dots]_{\gamma^1, \gamma^2} \longrightarrow \Gamma_N^2 \sum_{\gamma=\text{primitive}} B_\gamma^2 \sum_{p, p'=0}^{\infty} (1 - \Gamma_N)^{a(p+p')} \Gamma_S^{p+p'+c} [\dots]_{\gamma, p, p'}. \quad (27)$$

The exponents $a = 1$, $b = 0$ and $c = 1$ for class I, $a = 2$, $b = 0$ and $c = 0$ for class IIa and $a = 2$, $b = 2$ and $c = 2$ for class IIb are determined by the number of Andreev and normal reflections in Eqs. (22) and (24). Reflection phases do not appear because each time an electron is reflected at a tunnel barrier, a hole is reflected later. The argument in the double sum over p and p' in Eq. (27) has to be multiplied by the p - p' -dependent Andreev phase. The double sum over p and p' is easily resummed,

$$\sum_{p, p'=0}^{\infty} (1 - \Gamma_N)^{a(p+p')+b} \Gamma_S^{p+p'+c} e^{i(p-p')(\phi-\pi)} = \quad (28)$$

$$\frac{\Gamma_S^c (1 - \Gamma_N)^b}{1 - 2\Gamma_S (1 - \Gamma_N)^a \cos[\pi - \phi] + \Gamma_S^2 (1 - \Gamma_N)^{2a}}.$$

We next evaluate $\sum_\gamma B_\gamma^2$ by relating it to classical transmission probabilities [29]. Because the sum runs over primitive trajectories whose stability is given by their

electronic (or hole) component alone, one considers that the cavity is opened to four normal leads. The sum runs over all trajectories such as those sketched in Fig. 6. For class I, these trajectories are made up of two legs, both of them starting at y_0 on the L lead, and we write $\sum B_\gamma^2 = \sum_{\gamma^1, \gamma^3} B_{\gamma^1}^2 B_{\gamma^3}^2$. The leg γ^1 makes a normal angle θ_0 with respect to the normal to a cross-section of L and ends up in lead S_1 , while γ^3 makes a normal angle $\theta'_0 = -\theta_0$ and goes to lead S_2 . Both incidence position and angle on S_1 and S_2 have to be integrated over.

We define $P(\mathbf{Y}, \mathbf{Y}_0; t) \delta y \delta \theta \delta t$ as the classical probability to go from an initial position and momentum angle $\mathbf{Y}_0 = (y_0, \theta_0)$ on a lead to within $(\delta y, \delta \theta)$ of $\mathbf{Y} = (y, \theta)$ on another lead, in a time within δt of t . The sum over all primitive trajectories of class I can then be rewritten

as

$$\begin{aligned}
\sum_{\gamma, \text{primitive}} B_\gamma^2 &= p_F \int_0^{\tau_E} dt_{s1} \int_0^{\tau_E - t_{s1}} dt_{s3} \int_{-\pi/2}^{\pi/2} d\theta_0 d\theta'_0 \\
&\times \int_{S1} dy_{s1} \int_{S2} dy_{s3} \int_{-\pi/2}^{\pi/2} d\theta_{s1} d\theta_{s2} \\
&\times P(\mathbf{Y}_{s1}, \mathbf{Y}_0; t_{s1}) P(\mathbf{Y}_{s3}, \mathbf{Y}_0; t_{s3}) \\
&\times \cos \theta_0 \cos \theta'_0 \delta(\theta_0 + \theta'_0) \delta(y_0 - y'_0). \quad (29)
\end{aligned}$$

The factor $p_F \cos \theta_0$ measures the injected current, and since electrons are reflected (and not injected) at the L tunnel barrier, one has an additional $\cos \theta'_0$ (instead of $p_F \cos \theta'_0$). For a given cavity, P is a sum of δ -functions over all possible classical trajectories. Instead we consider the distribution averaged over a mesoscopic ensemble of similar cavities or a small energy interval. This gives a smooth function

$$\langle P(\mathbf{Y}_{si}, \mathbf{Y}; t) \rangle = \frac{\tau_{D,S}^{-1} \cos \theta_{si}}{4(\Gamma_N W_N + \Gamma_S W_S)} \exp[-t/\tau_{D,S}], \quad (30)$$

where $W_{N,S} = N_{N,S} \pi / k_F$ gives the width of the normal and superconducting leads. We insert (30) into (29), and perform the integrals. Combining the result with Eqs. (20), (27) and (28) delivers the resonant semiclassical contribution to T_{LL}^{he} ,

$$\begin{aligned}
\langle T_{LL}^{he} \rangle_r &= \frac{\pi \Gamma_N^2 N_N}{4} \left(\frac{N_S}{2\Gamma_N N_N + 2\Gamma_S N_S} \right)^2 \\
&\times \left(1 - (1 + \tau_E/\tau_{D,S}) \exp[-\tau_E/\tau_{D,S}] \right) \\
&\times \frac{\Gamma_S}{1 - 2\Gamma_S (1 - \Gamma_N) \cos[\pi - \phi] + \Gamma_S^2 (1 - \Gamma_N)^2}. \quad (31)
\end{aligned}$$

The semiclassical contribution to T_{RL}^{ee} arises from class II trajectories. The geometry is detailed in Fig. 6, and a similar calculation as above delivers

$$\begin{aligned}
\langle T_{RL}^{ee} \rangle_r &= \frac{\pi^2 \Gamma_N^2 N_N^2}{8N_S} \left(\frac{N_S}{2\Gamma_N N_N + 2\Gamma_S N_S} \right)^3 \\
&\times \left(1 - (1 + \tau_E/\tau_{D,S} + \tau_E^2/2\tau_{D,S}^2) \exp[-\tau_E/\tau_{D,S}] \right) \\
&\times \frac{1 + \Gamma_S^2 (1 - \Gamma_N)^2}{1 - 2\Gamma_S (1 - \Gamma_N)^2 \cos[\pi - \phi] + \Gamma_S^2 (1 - \Gamma_N)^4}. \quad (32)
\end{aligned}$$

The semiclassical contribution to the conductance is given by the sum of Eqs. (31) and (32). It clearly exhibits the functional dependence of resonant tunneling, where the resonance is however always at the Fermi level, and is achieved by setting the phase difference between the two superconductors at $\phi = \pi$. This resonance condition is the same for all semiclassical contributions we just discussed. This is why the resonance is macroscopic, giving a conductance $G \propto N_N$ and not of order one, as is usually the case for resonant tunneling. We also see that the effect disappears if the superconductors are poorly connected to the normal cavity, $\Gamma_S \rightarrow 0$, as should be.

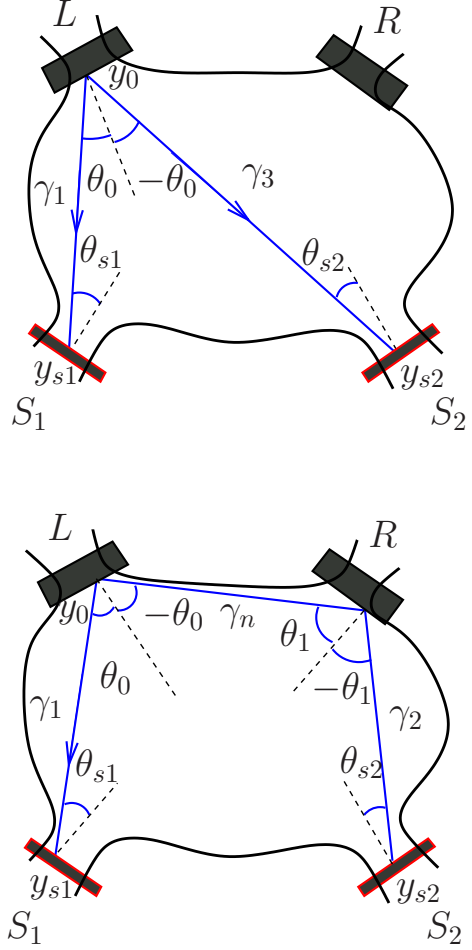


Figure 6: The effective four-terminal cavity used in the calculation of $\sum B_\gamma^2$, and the geometry of class I (top panel) and class II (bottom panel) trajectories.

Comparing Eqs. (31) and (32) to Eq. (13) we see that semiclassical contributions matter only close to resonance. In the tunneling regime, they increase the conductance by a factor $\propto \Gamma_N^{-1}$, from $G(\pi)/G_0 \propto \Gamma_N N_N$ to $G(\pi)/G_0 \propto N_N$, resulting in a peak-to-valley ratio of the conductance $G(\phi = \pi)/G(\phi = 0) \propto \Gamma_N^{-2}$. In most instances, $\langle T_{LL}^{eh}(\pi) \rangle_r \gg \langle T_{RL}^{ee}(\pi) \rangle_r$, and the sharpness of the resonance peak, measured by its width at half height, is proportional to Γ .

IV. NUMERICAL SIMULATIONS

We compare our theory with numerical simulations on a quantum mechanical model of the Andreev billiard, the Andreev kicked rotator [12].

A. The Andreev kicked rotator

One-dimensional maps give a stroboscopic description of dynamical systems. An example is the kicked rotator, describing the dynamics of a particle confined to a circle which is kicked periodically in time with period τ_0 and a kicking strength depending on its position [8]. The quantized version of this map is characterized by its Floquet operator, the unitary operator giving the time-evolution from one kick to the next, i.e. from time t to $t + \tau_0$. We represent the Floquet operator as a $M \times M$ matrix with matrix elements (from now on we measure times in units of $\tau_0 \equiv 1$)

$$F_{nm} = e^{-(i\pi/2M)(n^2+m^2)}(UQU^\dagger)_{nm}, \quad (33a)$$

$$U_{nm} = M^{-1/2}e^{(2\pi i/M)nm}, \quad (33b)$$

$$Q_{nm} = \delta_{nm}e^{-(iMK/2\pi)\cos(2\pi n/M)}. \quad (33c)$$

Here K is the kicking strength. For $K \gtrsim 7$ the classical dynamics is chaotic, with classical Lyapunov exponent $\lambda \simeq \ln[K/2]$. The eigenvalues of F are $e^{i\epsilon_m}$ ($m = 1 \dots M$), and the quasi-energies ϵ_m of the closed system (without any leads) have an average level spacing $\delta = 2\pi/M$. The dynamics of the electron is determined by F , while the time evolution of holes is given by F^* .

The kicked rotator model describes a closed system. We open it by inserting leads in a subspace of the Hilbert space, parametrized by the indices $\{m_1, m_2, \dots, m_{2N_N}\}$ for the normal leads and $\{l_1, l_2, \dots, l_{2N_S}\}$ for the superconducting leads. The coupling to the leads is described by a $2N_N \times M$ ($2N_S \times M$) projection matrix P_N (P_S) with matrix elements

$$[P_N]_{nm} = \begin{cases} \sqrt{\Gamma_N} & \text{if } m = n \in \{m_1, \dots, m_{2N_N}\}, \\ 0 & \text{otherwise,} \end{cases} \quad (34a)$$

$$[P_S]_{nm} = \begin{cases} \sqrt{\Gamma_S} & \text{if } m = n \in \{l_1, \dots, l_{2N_S}\}, \\ 0 & \text{otherwise.} \end{cases} \quad (34b)$$

The average time between Andreev reflections equals $\tau_{D,S} = M/2\Gamma_S N_S$. In our numerical investigations we restrict ourselves to $\Gamma_S = 1$. The Ehrenfest time of the closed Andreev billiard reads $\tau_E = \lambda^{-1} \ln(N_S^2/M)$ [9, 12].

We perform two sets of simulations, the first is devoted to the spectrum of a closed Andreev billiard, the second to the conductance through a chaotic Andreev interferometer.

1. The closed Andreev kicked rotator

Both electrons and holes have an energy near the Fermi energy, and therefore we assume that Andreev reflection is perfectly retroreflecting. The Floquet matrix of the Andreev billiard is then

$$\mathcal{F} = \mathcal{P}_S \begin{pmatrix} F & 0 \\ 0 & F^* \end{pmatrix}, \quad (35)$$

with

$$\mathcal{P}_S = \begin{pmatrix} 1 - P_S^T P_S & -iP_S^T e^{i\Phi} P_S \\ -iP_S^T e^{-i\Phi} P_S & 1 - P_S^T P_S \end{pmatrix}. \quad (36)$$

The coupling between electrons and holes is modelled by \mathcal{P}_S , which induces Andreev reflection for electron or holes touching the superconducting leads, i.e. induces transitions between the components $\{l_1, \dots, l_{2N_S}\}$ of the wavefunction in the two quasiparticle sectors. The phase difference between the two superconductors is contained in the $2N_S \times 2N_S$ matrix Φ , with elements $\delta_{nm}\phi/2$, for $n \leq N_S$ and $-\delta_{nm}\phi/2$ for $n > N_S$. The matrix \mathcal{F} can be diagonalized efficiently using the Lanczos technique in combination with the Fast-Fourier-Transform algorithm [42]. This allows to reach the large system sizes needed to explore the regime of finite Ehrenfest time.

2. The kicked Andreev interferometer

We first write the $(2N_N + 2N_S) \times (2N_N + 2N_S)$ energy-dependent scattering matrix of our four-terminal structure (without superconductor). It is related to the Floquet operator via [43]

$$S(\epsilon) = -(1 - PP^T)^{1/2} + P \frac{1}{e^{-i\epsilon} - F(1 - P^T P)} F P^T. \quad (37)$$

The $(2N_S + 2N_N) \times M$ coupling matrix

$$P = \begin{pmatrix} P_N & 0 \\ 0 & P_S \end{pmatrix}, \quad (38)$$

describes coupling to all four leads. The four-terminal scattering matrix S is made of sixteen sub-blocks S_{ij} , where the subindices $i, j = L, R, S1$ and $S2$ label either normal or superconducting terminals. From these sub-blocks, the exact expression for the conductance, Eq. (16), can be computed, following Ref. [25]. The transmission amplitudes giving the probabilities in Eq. (17) can be written as

$$\tau^{ee} = a - b\Omega c^* \Omega^* (1 + c\Omega c^* \Omega^*)^{-1} d, \quad (39a)$$

$$\tau^{he} = -ib^* \Omega^* (1 + c\Omega c^* \Omega^*)^{-1} d, \quad (39b)$$

in terms of the matrices

$$a = \begin{pmatrix} S_{L,L} & S_{L,R} \\ S_{R,L} & S_{R,R} \end{pmatrix}, \quad b = \begin{pmatrix} S_{L,S1} & S_{L,S2} \\ S_{R,S1} & S_{R,S2} \end{pmatrix},$$

$$c = \begin{pmatrix} S_{S1,S1} & S_{S1,S2} \\ S_{S2,S1} & S_{S2,S2} \end{pmatrix}, \quad d = \begin{pmatrix} S_{S1,L} & S_{S1,R} \\ S_{S2,L} & S_{S2,R} \end{pmatrix},$$

$$\Omega = \begin{pmatrix} e^{-i\phi/2} & 0 \\ 0 & e^{i\phi/2} \end{pmatrix}.$$

For numerical stability and efficiency, the transmission matrices τ of Eqs. (39) are constructed from self-consistent linear equations for the output amplitudes as a function of unity input on each N_N channel, one at a time, and not via direct inversion.

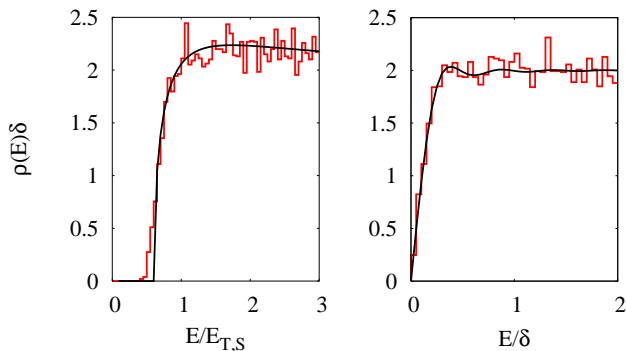


Figure 7: Left panel: density of states for the Andreev kicked rotator with $\phi = 0$, $M = 2048$, $N_S = 25$, $K = 147$, $\Gamma_S = 1$. The solid line gives the prediction of Eqs. (3) and (4). Data are averaged over 50 different lead positions. Right panel: density of states for the Andreev kicked rotator with $\phi = \pi$, $M = 2048$, $N_S = 25$, $\Gamma_S = 1$. The solid line gives the prediction of Eq. (5). Data are averaged over 50 different lead positions and 50 values of the kicking strength $K \in [144.5, 147.5]$

B. Numerics in the universal regime

We start with a comparison of the analytical predictions of RMT with numerical results, by choosing the parameters of the Andreev kicked rotator in such a way that $\tau_E \ll \tau_{D,S}$. In Fig. 7 we show the density of states for $\phi = 0$ and $\phi = \pi$. We compare our results with the theoretical predictions of Eqs. (3) and (4) for $\phi = 0$, while for $\phi = \pi$ we use Eq. (5). In both cases we find perfect agreement between numerics and RMT predictions.

We next turn our attention to the conductance. We choose an Andreev billiard with the same parameters as in Fig. 7, but couple it to normal leads. The conductance as a function of the phase difference is shown in Fig. 8. The numerical results, for several values of the parameters Γ_N and N_N (characterizing the normal leads), are compared with the circuit theory prediction of Eqs. (11) and (12). The agreement is excellent. In the tunneling limit $\Gamma_N \rightarrow 0$ the conductance is strongly suppressed for $\phi \neq \pi$ while it is restored to its value in absence of superconductor when $\phi = \pi$, as predicted by Eq. (13).

In Fig. 9, we show the conductance as a function of Γ_N , both for $\phi = 0$ and $\phi = \pi$. For $\phi = 0$ the circuit theory of Eqs. (11) and (12) (solid lines) predict a curve that depends only on the ratio $\alpha \equiv N_S/N_N$. The numerical data line up on the analytical curves. For $\phi = \pi$ the analytical prediction of circuit theory coincides with the conductance of the billiard in the absence of superconductors i.e. $G/G_0 = \Gamma_N N_N/2$. As $\Gamma_N N_N$ is reduced, however, the data deviate from this prediction. We attribute this to the fact that the circuit theory results are accurate to leading order in $\Gamma_N N_N$ only. This argument is corroborated by the fact that the data for the largest N_N remain close to the circuit theory prediction down to lower values of Γ_N .

We next present in Fig. 10 data for the conductance

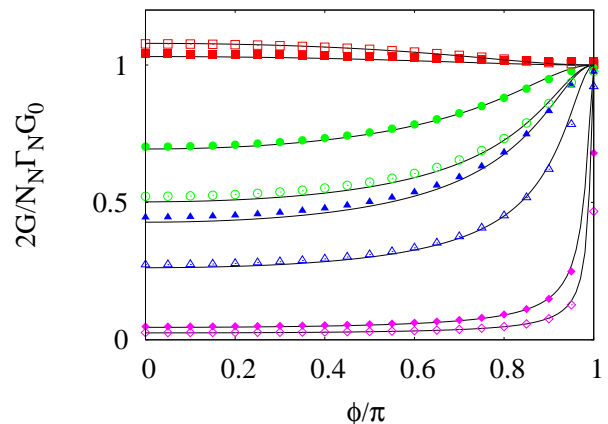


Figure 8: Conductance of the Andreev kicked rotator as a function of the phase difference ϕ between the two superconductors. For all curves $M = 2048$, $N_S = 25$, $K = 147$. The closed symbols correspond to $N_N = 100$ and the open symbols to $N_N = 50$, with $\Gamma_N = 1$ (squares), $\Gamma_N = 0.2$ (circles), $\Gamma_N = 0.1$ (triangles) and $\Gamma_N = 0.01$ (diamonds). The solid lines are the relevant predictions from circuit theory. Every data point is an average over 200 realizations.

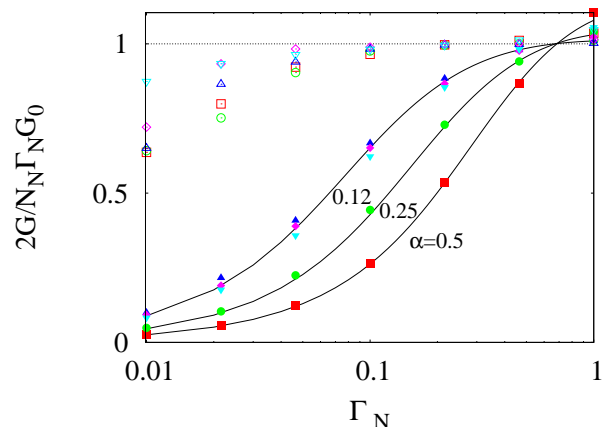


Figure 9: Conductance of the Andreev kicked rotator as a function of Γ_N for $K = 147$, $M = 2048$, $\Gamma_S = 1$, at $\phi = 0$ (closed symbols) and $\phi = \pi$ (open symbols), and $N_N/N_S = 100/50$ (squares), $100/25$ (circles), $100/12$ (upward pointing triangles), $200/25$ (diamonds) and $400/50$ (downward pointing triangles). Every data point is an average over 50 realizations. The solid lines are the predictions from circuit theory for $\phi = 0$ and $\alpha = N_S/N_N = 0.5, 0.25$, and $\alpha = 0.12$, while the dashed line corresponds to $\phi = \pi$.

at finite excitation energy. For $\phi = \pi$, the conductance stays at its universal, $E = 0$ value, $G = \Gamma_N N_N/2$, independent of E . For $\phi = 0$ however, it increases from $G = \Gamma_N^2 N_N (1 + 2N_N/N_S)$ to $G = \Gamma_N N_N/2$ as E increases. The crossover occurs on the scale $\simeq 0.6E_{T,S}$ of the $\phi = 0$ Andreev gap (see the top panel of Fig. 7), which illus-

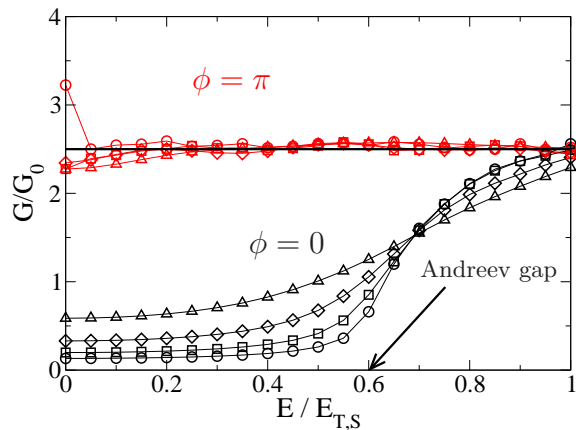


Figure 10: Transmission as a function of the normalized excitation energy $E/E_{T,S}$ for $M = 2048$, $N_N = 100$, $K = 147$, $\Gamma_N = 0.05$, at $\phi = 0$ (black symbols) and $\phi = \pi$ (red symbols) for $N_S = 25$ (triangles), 50 (diamonds), 100 (squares) and 200 (circles). The black curve shows the universal conductance at $\phi = \pi$ for $E = 0$.

trates further the connection between transport through the Andreev interferometer and the spectrum of the corresponding closed Andreev billiard. From the data in Fig. 10, we do not expect a fundamental departure from the zero-temperature theory in the universal regime, as long as the temperature lies below the Thouless energy, $T \lesssim E_{T,S}$. The situation is different in the semiclassical regime, which can already be inferred from the $N_S = 200$ data presented in Fig. 10. Despite a rather small ratio $\tau_E/\tau_{D,S} \approx 0.13$, this set of data already exhibits a peak at $E = 0$ above the universal conductance for $\phi = \pi$. This peak however quickly disappears with $E \ll E_{T,S}$.

We finally stress that for the data presented in Figs. 7–8 and 9, $\tau_E/\tau_{D,S} < 0.02$. We found that, to get a good agreement between our numerics and RMT predictions at $\phi = \pi$, it is necessary to set $\tau_E/\tau_{D,S}$ to much smaller values than in our earlier numerical works with $\phi = 0$ [12, 13, 15]. This is especially true for the density of states at $\phi = \pi$ (where we needed to go down to $\tau_E/\tau_{D,S} \approx 10^{-3}$), and is already a good indication that the semiclassical effect at $\phi = \pi$ is much larger than the manifestations of Ehrenfest physics investigated so far.

C. Semiclassical limit

We next investigate the spectrum of closed Andreev billiard at finite $\tau_E/\tau_{D,S}$. Density of states of closed billiards are shown in Fig. 11. The density of states is only weakly dependent on $\tau_E/\tau_{D,S}$ at $\phi = 0$ (left panel). At $\phi = \pi$ however, the semiclassical regime sees the emergence of a giant peak in the density of states at the Fermi energy (right panel).

In Fig. 12, we next show a conductance resonance curve in the semiclassical regime. We obtain very good agree-

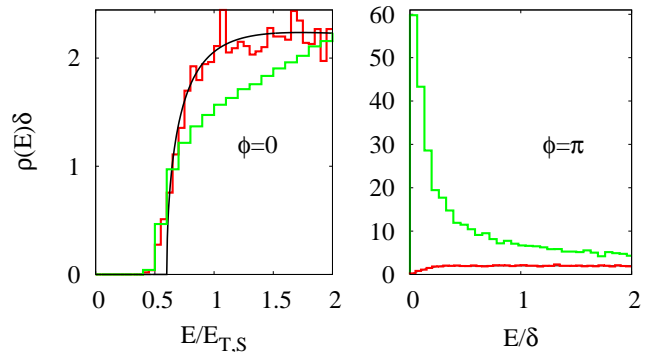


Figure 11: Density of states of closed Andreev billiards, for $\phi = 0$ (left panel) and $\phi = \pi$ (right panel), in the universal regime with $M = 2048$, $N_S = 25$ and $K = 148$ (red curves, $\tau_E/\tau_{D,S} = 0$, data averaged over 2500 samples) and in the semiclassical regime with $M = 8192$, $N_S = 800$ and $K = 10$ (green curves, $\tau_E/\tau_{D,S} = 0.55$, 500 samples). The black curves indicate the universal predictions [4, 35]. Note the different horizontal and vertical scales.

ment between the numerical data (circles) and the analytical prediction (green solid line) with $\tau_E/\tau_{D,S} \simeq 0.79$. Without the semiclassical contribution, the universal prediction of Eqs. (11–12) in the full range $\phi \in [0, 2\pi]$ is given by the red line. While the latter fits the resonance curve far away from resonance, the agreement breaks down close to $\phi = \pi$, where universal contributions give a prediction $G(\pi) = 2G_0$, too small by an order of magnitude. The left inset in Fig. 12 illustrates the increase of the peak height and narrowness as the semiclassical parameter M increases. The four sets of data in this inset correspond to a fixed set of classical parameters, with the electronic wavelength decreasing by factors of four from one curve to the next, starting from the bottommost (blue) curve. The conductance increases at each step because the number of conduction channels scales linearly with M . In absence of semiclassical contributions, these four curves would exhibit the same peak-to-valley ratio, but here they do not. This is quantified in the right inset to Fig. 12, where we show both the peak height and the peak-to-valley ratio corresponding to the same classical configuration as in the main plot, while varying M .

We can connect the data in Figs. 11 and 12, since they correspond to the same closed Andreev billiard. The broadening of levels due to the external normal leads is $\delta E \simeq \Gamma_N N_N \delta / 2\pi$. For the resonance in Fig. 12, this gives $\delta E = 2\delta/\pi$. From the green curve in Fig. 11, we estimate that this value of δE covers about 20 to 30 levels around the Fermi energy. Those states condense on classical orbits bouncing on average $M/2N_S = 5$ times at the billiard’s boundary. At each bounce, they have a probability $\simeq 1 - 2N_N/(M - 2N_S)$ not to touch a normal lead. Therefore, since $[1 - 2N_N/(M - 2N_S)]^5 \approx 1/2$ for the data in Fig. 12 with $N_N = 400$ channels, we estimate that about half of these 20–30 states couple to the leads. One thus expects a resonant contribution to

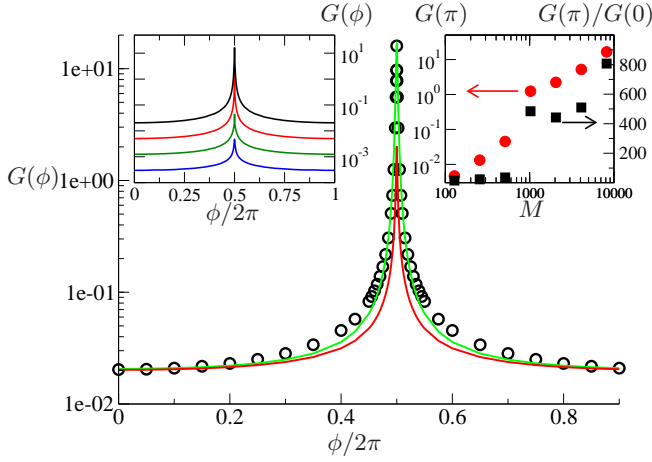


Figure 12: Conductance through a chaotic Andreev interferometer vs. the phase difference ϕ between the two superconductors. Circles are numerical results obtained from the Andreev kicked rotator with $\Gamma_N = 0.01$, $M = 8192$, $M/N_N = 20$, $M/N_S = 10$ and $K = 10$. The green curve is the analytical prediction obtained by summing the semiclassical resonant contributions with the universal prediction. The red curve gives the universal prediction obtained from circuit theory. Left inset: Numerical data for the same classical parameters $M/N_N = 20$, $M/N_S = 10$ and $K = 10$ as in the main plot, for $M = 128$ (blue curve), 512 (green curve), 2048 (red curve), to 8192 (black curve). Note the change in peak-to-valley ratio. Right inset: peak-to-valley ratio $G(\pi)/G(0)$ (black squares) and peak conductance $G(\pi)$ (red circles) as a function of M controlling the quantum-to-classical crossover, for the same classical configuration as in the main plot. Data are averaged over 150–1000 sample realizations.

the conductance $\sim 10 - 15G_0$, which agrees quite well with the numerical value of $G(\pi) \simeq 16G_0$ for the data of Fig. 12, with a universal contribution of $2G_0$.

In Fig. 13 we show the conductance as a function of the number of channels in each superconducting lead N_S , for two different values of Γ_N . We see that the conductance depends strongly on N_S , in contrast to the RMT prediction $G = G_0\Gamma_N N_N/2$ which is independent of it. In the parameter range of the figures, the contribution of Eq. (32) can be neglected and the contribution of Eq. (31) dominates. For $\phi = \pi$ and $\Gamma_N \rightarrow 0$, it can be simplified to $T_{LL}^{he} = (\pi N_N/16)(1 - (1 + \tau_E/\tau_{D,S})\exp[-\tau_E/\tau_{D,S}])$. This contribution depends strongly on N_S since both the Ehrenfest time and the time $\tau_{D,S}$ between Andreev reflections depend on N_S . It is therefore the relative measure of trajectories of class I which causes the order-of-magnitude increase of conductance with N_S observed in Fig. 13. The solid lines give the theoretical prediction obtained by summing the semiclassical resonant contribution, Eqs. (31) and (32), and the universal contribution obtained from Eqs. (11) and (12). There is good agreement between the numerical data and the theory, as long as the superconducting dwell time is long enough. For $N_S > 400$, $\tau_{D,S} < 5$, and we suspect that short processes across the billiard increase the conductance well above

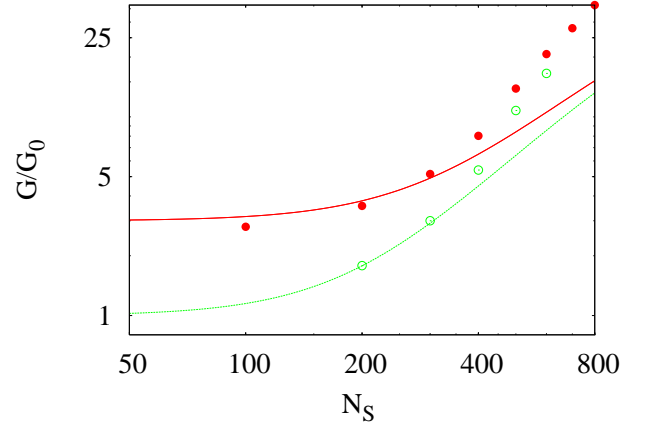


Figure 13: The conductance of the Andreev kicked rotator as a function of N_S for $K = 10$, $M = 4096$, $\Gamma_S = 1$, $\phi = \pi$, $N_N = 200$ and $\Gamma_N = 0.03$ (closed circles), $\Gamma_N = 0.01$ (open circles). Every data point is an average over at least 80 realizations. The lines represent a sum of the semiclassical prediction Eq. (31) in the tunneling limit and the RMT result of Eq. (13) for $\Gamma_N = 0.03$ (solid red line) and $\Gamma_N = 0.01$ (dashed green line).

the analytical prediction.

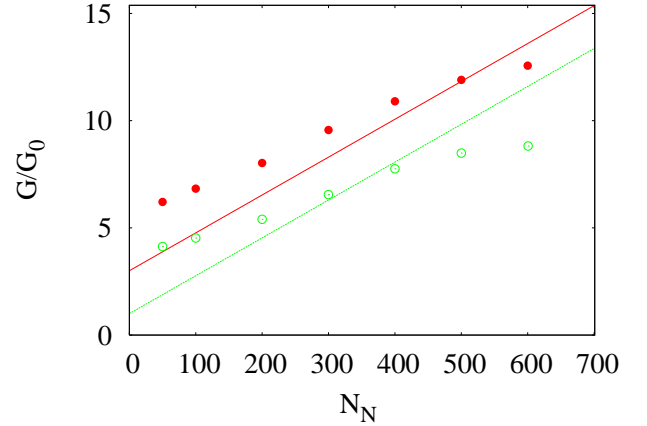


Figure 14: The conductance of the Andreev kicked rotator as a function of N_N for $K = 10$, $M = 4096$, $N_S = 400$, $\Gamma_S = 1$, $\phi = \pi$ and $\Gamma_N = 6/N_N$ (closed circles), $\Gamma_N = 2/N_N$ (open circles). Every data point is an average over at least 80 realizations. The lines represent a sum of the semiclassical prediction Eq. (31) in the tunneling limit and the universal RMT result of Eq. (13) or $\Gamma_N = 6/N_N$ (solid red line) and $\Gamma_N = 2/N_N$ (dashed green line).

Finally, we show on Fig. 14 the conductance as a function of N_N . The product $\Gamma_N N_N$ is kept constant, so that any observed N_N dependence arises from nonuniversal effects. Even though we always have moderate Ehrenfest times $\tau_E < \tau_{D,S}$, the numerical results are very different from the constant conductance predicted in the universal

regime. The semiclassical contributions dominate and we see an increase of G with N_N . Here, $\tau_E/\tau_{D,S} \simeq 0.6$ is constant, and the increase of the conductance is predicted to be linear, see Eqs. (31) and (32). There is reasonable agreement between theory and numerical data, with significant deviations in the regime of small N_N , where we leave the tunneling regime.

We conclude that our numerical data fully confirm our analytical results.

V. CONCLUSION

We have presented analytical and numerical investigations of spectroscopy and transport in quantum chaotic Andreev billiards coupled to two superconductors. We identified two regimes with very different behaviors. In the universal regime, the presence of the superconductor opens up a gap in the density of states of the Andreev billiard at the Fermi level, which reduces the conductance through the system once it is attached to two external normal leads with tunnel contacts. This gap closes when the phase difference between the two superconductors is $\phi = \pi$, and in the tunneling limit, the normal conductance that the system would have in the absence of superconductivity is recovered. As the Fermi wavelength is reduced, λ_F/W_S , $\lambda_F/L_c \ll 1$, one enters a new, semiclassical regime, where the situation is only marginally different unless the phase difference between the two superconductors is close to π . When this is the case, we found an order-of-magnitude enhancement of the tunneling conductance, and identified the mechanism behind this enhancement as resonant tunneling through a macroscopic number of quasi-degenerate levels at the Fermi energy of the corresponding closed Andreev billiard.

Our calculation focused on the zero-temperature limit of transport, and we finally comment on the effect of a finite temperature. From Fig. 10, we concluded that, in the universal regime, the shape of the conductance oscillations do not differ from those presented in Fig. 8, as long as the temperature lies below the superconducting

Thouless energy, $E_{T,S} = \Gamma_S N_S \delta / 2\pi$. The semiclassical contribution to the conductance near $\phi = \pi$ is however much more sensitive to changes in temperatures than the universal one. Finite excitation energies indeed lead to an additional action phase accumulated along transport orbits. The expressions in Eqs. (26) and (28) are now combined into the following expression

$$\frac{1}{\tau_{D,S}^2} \sum_{p,p'=0}^{\infty} (1 - \Gamma_n)^{a(p+p')+b} \Gamma_s^{p+p'+c} e^{i(p-p')(\phi-\pi)} \quad (40)$$

$$\times \int_0^{\tau_E} dt_{s1} \int_0^{\tau_E - t_{s1}} dt_{s3} e^{-[t_{s1} + t_{s3}][\tau_{D,S}^{-1} + iE(p-p')/\hbar]}.$$

The accumulation of an E -dependent action phase results in a cut-off for the summation over p and p' , effectively suppressing contribution with $p - p' \gtrsim p_{\max}^{(-)} \equiv (\hbar/E \tau_{D,S})^2$. One ends up with a prefactor $1 - (1 - \Gamma_N)^{p_{\max}^{(-)}}$ multiplying Eqs. (31) and (32), which suppresses the semiclassical contribution already for temperatures significantly smaller than $E_{T,S}$. At finite temperature, the resonant conductance enhancement discussed above will thus be maximal for an intermediate value of Γ_N optimizing macroscopic resonant tunneling while minimizing thermal averaging.

Acknowledgments

We thank C. Beenakker for drawing our attention to Refs. [21, 26], M. Büttiker for helpful and valuable comments, and A. Kadigrobov for pointing out Ref. [22] and for a brief discussion on Refs. [21, 22]. M. Goorden was supported by the EU Marie Curie RTN "Fundamentals of Nanoelectronics", MCRTN-CT-2003-504574. P. Jacquod expresses his gratitude to M. Büttiker and the Department of Theoretical Physics at the University of Geneva for their hospitality during the summer of 2007.

-
- [1] A. F. Andreev, Zh. Eksp. Teor. Fiz. **46**, 1823 (1964) [Sov. Phys. JETP **19** 1228 (1964)].
 - [2] Y. Imry, *Introduction to Mesoscopic Physics* (Oxford University, Oxford, 2002); B.J. van Wees and H. Takayanagi, in *Mesoscopic Electron Transport*, L.L. Sohn, L.P. Kouwenhoven and G. Schön Eds., NATO ASI Series E345 (Kluwer, Dordrecht, 1997).
 - [3] I. Kosztin, D. L. Maslov, and P. M. Goldbart, Phys. Rev. Lett. **75**, 1735 (1995).
 - [4] J. A. Melsen, P. W. Brouwer, K. M. Frahm, and C. W. J. Beenakker, Europhys. Lett. **35**, 7 (1996).
 - [5] H. Schomerus and C. W. J. Beenakker, Phys. Rev. Lett. **82**, 2951 (1999).
 - [6] O. Bohigas, M. J. Giannoni, and C. Schmit, Phys. Rev. Lett. **52**, 1 (1984); S. Müller, S. Heusler, P. Braun P, F. Haake, and A. Altland, Phys. Rev. Lett. **93**, 014103 (2004).
 - [7] A. Lodder and Yu. V. Nazarov, Phys. Rev. B **58**, 5783 (1998).
 - [8] H. Schomerus and Ph. Jacquod, J. Phys. A. **38**, 10663 (2005).
 - [9] M. G. Vavilov and A. I. Larkin, Phys. Rev. B **67**, 115335 (2003).
 - [10] İ. Adagideli and C. W. J. Beenakker, Phys. Rev. Lett. **89**, 237002 (2002).
 - [11] P. G. Silvestrov, M. C. Goorden, and C. W. J. Beenakker, Phys. Rev. Lett. **90**, 116801 (2003).
 - [12] Ph. Jacquod, H. Schomerus, and C. W. J. Beenakker,

- Phys. Rev. Lett. **90**, 207004 (2003).
- [13] M. C. Goorden, Ph. Jacquod, and C. W. J. Beenakker, Phys. Rev. B **68**, 220501(R) (2003).
- [14] A. Kormányos, Z. Kaufmann, C.J. Lambert, and J. Cserti, Phys. Rev. B **70**, 052512 (2004).
- [15] M. C. Goorden, Ph. Jacquod, and C. W. J. Beenakker, Phys. Rev. B **72**, 064526 (2005).
- [16] P.G. Silvestrov, Phys. Rev. Lett. **97**, 067004 (2006).
- [17] J. A. Melsen, P. W. Brouwer, K. M. Frahm, and C. W. J. Beenakker, Physics Scripta **T69**, 223 (1997).
- [18] F. Zhou, P. Charlat, B. Spivak, and B. Pannetier, J. Low Temp. Phys. **110**, 841 (1998).
- [19] D. Taras-Semchuk and A. Altland, Phys. Rev. B **64**, 014512 (2001).
- [20] C. W. J. Beenakker, Rev. Mod. Phys. **69**, 731 (1997).
- [21] A. Kadigrobov, A. Zagroskin, R.I. Shekhter, and M. Jonson, Phys. Rev. B **52**, R8662 (1995). This article makes the unphysical assumption that the interferometer does not mix transport modes and therefore acts as N identical one-dimensional interferometers in parallel.
- [22] H.A. Blom, A. Kadigrobov, A.M. Zagroskin, R.I. Shekhter, and M. Jonson, Phys. Rev. B **57**, 9995 (1998). In this article, the chaoticity of the cavity is related to the strength of the tunnel barriers between the leads and the cavity in such a way that, in the tunneling limit, $\Gamma_N \ll 1$, the cavity becomes regular.
- [23] B.Z. Spivak and D.E. Khmel'nitskii, JETP Lett. **35**, 412 (1982). This work lies somehow outside our present focus, as it considers temperatures larger than $E_{T,S}$.
- [24] A.V. Zaitsev, Phys. Lett. A **194**, 315 (1994).
- [25] C.W.J. Beenakker, J.A. Melsen, and P.W. Brouwer, Phys. Rev. B **51**, 13883 (1995).
- [26] A. Kadigrobov, L.Y. Gorelik, R.I. Shekhter, and M. Jonson, Superlattices and Microstructures **25**, 961 (1999).
- [27] Y. V. Nazarov, Phys. Rev. Lett. **73**, 1420 (1994).
- [28] N. Argaman, Europhys. Lett. **38**, 231 (1997).
- [29] Ph. Jacquod and R. S. Whitney, Phys. Rev. B **73**, 195115 (2006).
- [30] K. Richter and M. Sieber, Phys. Rev. Lett. **89**, 206801 (2002); S. Heusler, S. Müller, P. Braun, and F. Haake, Phys. Rev. Lett. **96**, 066804 (2006).
- [31] Í. Adagideli, Phys. Rev. B **68**, 233308 (2003).
- [32] P. W. Brouwer and S. Rahav, Phys. Rev. B **74**, 075322 (2006).
- [33] R.S. Whitney, Phys. Rev. B **75**, 235404 (2007).
- [34] K.M. Frahm, P.W. Brouwer, J.A. Melsen, and C.W.J. Beenakker, Phys. Rev. Lett. **76**, 2981 (1996).
- [35] A. Altland and M. R. Zirnbauer, Phys. Rev. B **55**, 1142 (1997).
- [36] W. Ihra, M. Leadbeater, J.L. Vega, and K. Richter, Eur. Phys. J. B **21**, 425 (2001); O. Zaitsev, J. Phys. A **39**, L467 (2006).
- [37] S. Iida, H.A. Weidenmüller, and J.A. Zuk, Phys. Rev. Lett. **64**, 583 (1990).
- [38] C.J. Lambert, J. Phys. Cond. Mat. **5**, 707 (1993); N. R. Claughton and C. J. Lambert, Phys. Rev. B **53**, 6605 (1996).
- [39] L. Couchman, E. Ott, and T.M. Antonsen, Phys. Rev. A **46**, 6193 (1992).
- [40] The segments γ_{si} , $i = 1, 2, 3$ in Fig.5 might include many intermediate bounces at a tunnel barrier. All possible number of reflections are effectively resummed; see Ref. [33] for more details.
- [41] F. Haake, *Quantum Signatures of Chaos*, 2nd Ed. Springer, Berlin (2001).
- [42] R. Ketzmerick, K. Kruse, and T. Geisel, Physics D **131**, 247 (1999).
- [43] Y. V. Fyodorov and H.-J. Sommers, JETP Lett. **72**, 422 (2000).
- [44] J. Tworzydło, A. Tajic and C. W. J. Beenakker, Phys. Rev. B **68**, 115313 (2003).